https://dx.doi.org/10.22161/ijaers.6.2.20 ISSN: 2349-6495(P) | 2456-1908(O)

Synthesis, characterization and photocatalytic activity of activated charcoal prepared from vegetable sponge for photocatalytic degradation of Rhodamine B dye

Karolina Marques Enick[1], Luís Otávio Bulhões[1], Cristiane dos Santos[2], Luís Fernando Wentz Brum[2],William Leonardo da Silva[1*]

[1]Universidade Franciscana
Rua Silva Jardim nº 1323, 97010-491, Santa Maria - RS, Brasil
[2] Instituto de Química – Universidade Federal do Rio Grande do Sul
Av. Bento Gonçalves n° 9500, 91501-970, Porto Alegre – RS, Brasil

*Corresponding author. *Phone*: +55 55 30266971
E-mail address: williamleonardo_silva@hotmail.com(W.L. da Silva).

***Abstract*—** *An alternative for the correct treatment and final disposal of these wastes are the Advanced Oxidative Processes, in particular heterogeneous photocatalysis. Thus, the vegetable sponge (Luffa cylindrica) was used for the synthesis of activated carbon and photocatalysts doped with TiO_2, for application in heterogeneous photocatalysis. The samples were characterized by diffuse reflectance spectroscopy (DRS-UV), nitrogen porosimetry, zeta potential (ZP) and scanning electron microscopy (SEM). To evaluate the photocatalytic activity, experiments were carried out in a stirred batch reactor, with the photocatalyst in suspension, under ultraviolet and visible radiation and as the target molecule was used the rhodamine B dye. The doped photocatalyst with Ti^{+4} synthesized from the activated carbon prepared with sucrose and glycine showed the best photocatalytic activity in the degradation of the RhB dye of 66 % ($k = 0.0088\ min^{-1}$, under ultraviolet radiation) and 49.8 % ($k = 0.0059\ min^{-1}$, under visible radiation) after 120 minutes of the reaction, while, under the same conditions, the commercial catalyst P25 showed a degradation of 53.92 % and 40.44 %, respectively.*

***Keywords*— Dyes; Heterogeneous photocatalysis; Titanium doping; Vegetable sponge; Degradation.**

I. INTRODUCTION

The growing urbanization and industrialization of society have reflected an increase in the generation of wastes, whether domestic or industrial, and its inadequate disposal has caused a serie of serious environmental damages (Dunn, 2012). Thus, considering that there is a fine line between the human development and water quality, it is indispensable to maintenance of good quality of the water sources to there is a full economic development and ensure health care of the population.

In addition, wastes from industrial and agricultural activities constitute a large part of the amount of toxic or rich residues in microbial activity that are currently generated(Mourão and De Mendonça, 2009). Moreover, despite the fact that Brazil is the pioneer in the development of regulatory standards for the disposal of liquid effluents, these wastes still constitute a major public health problem (Almeida *et al*., 2012).

At the same time, due to its physicochemical and biochemical characteristics, which may be biologically constituted, industrial wastes are destined to a receiving body, directly or indirectly, and can not be used economically or technically. Before this discharge, the constituents of these wastes must be treated according to sanitary, environmental and legal standards previously established in environmental legislation.

The treatment of effluents and industrial wastes is aimed at the preservation and integrity of the environment and receiving waters, as well as complying with norms and legislation on effluent emission standards. In this case, seeks to minimize and/ or avoid through different treatment technologies. Among these, stands out the Advanced Oxidative Processes (AOPs), technologies with the potential to oxidize a large variety of complex organic compounds (Ma *et al*., 2014), which are not removed by conventional sewage treatment processes.

In parallel, these methods are based on the action of a highly oxidizing species (the hydroxyl radical, •OH),

https://dx.doi.org/10.22161/ijaers.6.2.20 *ISSN: 2349-6495(P) | 2456-1908(O)*

which reacts with the various organic compounds, mineralizing them in non-toxic forms such as CO_2 and H_2O (Pereira *et al.*, 2010). Thus, the great advantage of AOPs is that, during the treatment of the organic compounds, they are destroyed and not only transferred from one phase to another, as in some conventional treatment processes. Among the AOPs, stands out the heterogeneous photocatalysis, a process that involves redox reactions induced by radiation on the surface of semiconductors (photocatalysts).

The ideal photocatalyst to heterogeneous photocatalysis should to have unique electronic and optical properties, high physical and chemical stability, low cost and non-toxicity (Liu *et al.*, 2011). However, some drawbacks of photocatalysts such as wide band gap energy and high rate of electron–hole recombination restricts its range of practical applications only under UV irradiation ($\lambda < 388$ nm) (Xu *et al.*, 2010; Lin *et al.*, 2011). Therefore, many research works have focused to extend its optical absorption edge from UV to the visible-light region and to decrease the electron–hole recombination rate. The prominent way to encounter these limitations is to alter the band gap energy via doping of some metals (e.g., Cu, Fe, Zn, Co, Mg, Al) and non-metals (e.g., N and Cl) (Zhang *et al.*, 2012; Wu *et al.*, 2011; Abed *et al.*, 2015).

Therefore, the present work aims to evaluate the potential of heterogeneous photocatalysts prepared from a vegetable sponge (*Luffa cylindrica*) in the form of activated carbon, evaluating the effect of doping with TiO_2 (Ti^{+4}) on the degradation of Rhodamine B dye (RhB) in aqueous solution under ultraviolet and visible radiation. For comparative reasons, commercial titania (Evonik Aeroxide P25) was also employed.

II. MATERIALS AND METHODS

2.1 Materials

Three combustible reagents were used to prepare the activated charcoal from vegetable sponge, such as glycine ($C_2H_5NO_2$, Vetec, 98,5%), sucrose ($C_{12}H_{22}O_{11}$, Labsytih, 99,95%) and urea (CH_4N_2O, CAQ, 99%). Rhodamine B ($C_{28}H_{31}ClN_2O_3$, Próton Química, P.A.) was used as the dye probe for the degradation tests. TiO_2 (Evonik Aeroxide P25). All other chemicals and reagents, being of analytical grade, were purchased from Merck (Germany) and used without further purification. Double-distilled deionized water was used for the preparation of the solutions used in the catalytic tests.

2.2 Synthesis of activated charcoal

Initially, the vegetable sponge was prepared, where it was manually cut, washed and dried (DeLeo 4400 W, Brazil) at 80 ºC for 12 hours. Afterwards, the combustion process occurred, where heat was generated through the heating elements, which was transferred to the surface of the sample. Finally, three different fuels (glycine, sucrose and urea) were used. Thus, three samples with different compositions of the fuels were prepared.

The combustion process was performed in muffle (Quimis Q318M, Brazil), where after carbonization, the material was macerated in order to obtain a fine and uniform texture. In addition, the method of synthesis of activated charcoal by combustion is characterized by being simple, producing high purity powders with high specific area and small particle size (Barros *et al.*, 2005).The labels that were employed are described in Table 1, which have been designated as x-A.C., where x refers to the fuels used in the synthesis.

Table.1: Compositions of activated charcoal (A.C.) in proportions

A.C.	vegetable sponge	sucrose	urea	glycine
SucGly-A.C.	0,422 g	0,900 g	0	0,200 g
Suc-A.C.	0,455 g	1,370 g	0	0
UreGly-A.C.	0,450 g	0	0,700 g	0,700 g

2.3 Synthesis of photocatalysts

The photocatalysts were synthesized by the doping of the activated charcoal with the photoactive metal precursor, in this case the TiO_2. Thus, for doping with Ti^{+4}, aqueous solutions were prepared using the activated charcoal (xA.C.) with titanium in the concentration of 25% w/w (Ti^{+4}/ xA.C.). Each solution was placed under continuous stirring at room temperature for 90 minutes and calcined at 450 ° C (heating rate 10 °C min^{-1}) for 4 hours. Photocatalysts doped with Ti^{+4} were labeled as xTi-A.C., where x refers to the different fuels, according to Table 2.

Table.2: Photocatalysts doped with Ti^{+4}

Sample	Label
A.C. + sucrose + glycine + TiO_2 (25 % w/w)	SucGlyTi-A.C.
A.C. + sucrose + TiO_2 (25 % w/w)	SucTi-A.C.
A.C. + urea + glycine + TiO_2 (25 % w/w)	UreGlyTi-A.C.

2.4 Characterization of photocatalyst

The specific surface area, pore diameter and pore volume of the samples were calculated from nitrogen measurements performed on a Micromeritics Gemini 2375 instrument. The energy band gap was determined by

https://dx.doi.org/10.22161/ijaers.6.2.20 ISSN: 2349-6495(P) | 2456-1908(O)

diffuse reflectance spectroscopy (DRS-UV) in a UV-visible spectrophotometer (Cary 100 Scan Spectrophotometers) equipped with an integrating sphere with a diameter of 60 mm using $BaSO_4$ as a standard. The scanning electron microscopy (SEM) was used to characterize the morphology of the photocatalysts using a scanning electron microscope-energy dispersive spectrometer X-ray JEOL model JSM 5800 operating between 5 and 20 and the samples were coated with a thin layer of conductive carbon by a sputtering technique. The zeta potential (ZP) was measured on a Malvern Zetasizer® nanoZS-style instrument.

2.5 Photocatalytic activity

Photocatalytic studies were performed in a 50 mL slurry reactor. In a typical reaction, 25 mL of the rhodamine B aqueous solution (9.58 M, pH ≅ 4.3) was introduced into the stirred tank reactor (STR) along with 0.0175 g of catalyst. The mixture was then stirred and illuminated with UV–visible light using a 125WHg vapor lamp (General Electric). The visible light source was a 125W mercury vapor lamp associated with a polycarbonate filter that excludes wavelengths below 385 nm. For the ultraviolet configuration, a similar lamp with a modified bulb was used. The radiation was adjusted to 202 W m^{-2} for the visible range (Pyranometer Type SL 100, Skilltech Instruments) and 61.8 W m^{-2} (Radiometer Series 9811, Cole-Parmer Instrument Company) for the UV range. The reaction temperature was maintained at 30 ± 2 ºC through continuous water circulation in the outer jacket of the STR. A blank phenol solution (without catalyst) was used as a control test. Then, the lamp was turned on, and an aliquot of the sample solution was withdrawn from the reactor at regular intervals (0, 5, 15, 30, 60, 75, 90 and 120 min). The photocatalyst was separated from the solution by centrifugation (Cientec CT-5000R) for 20 min at 5,000 rpm. The absorbance of the remaining dye in the solution was measured using a Varian Cary 100 UV-vis spectrophotometer (at a wavelength of 553 nm). The absorbance was correlated to the concentration of dye through a calibration curve where Abs = 0.0168 C (mg L^{-1}) (R^2 = 0.9911; n = 7). All of the photocatalytic tests were performedin duplicate (with error values less than 5%).

2.6 Photodegradation kinetics

Kinetics interpretations were conducted as a function of the remaining concentration of phenol in solution over time. Data were fitted as kinetic model of Langmuir-Hinshelwood (L-M)(Konstantinou and Albanis, 2004; Gaya and Abdullah, 2008; Herrmann, 2005), according to equation (1):

$$-r_i = -\frac{dC_i}{dt} = \frac{\kappa_S . K . C_i}{1 + K . C_i} \quad (1)$$

where κ_s is the true photodegradation rate of the organic compound, C_i the concentration of the compound, t the illumination time, and K the adsorption coefficient of the compound to be degraded. κ_s is related to several parameters such as mass of catalyst, efficient photon flow and layer of oxygen. The L–Hmodel can be simplified to a pseudo-first-order kinetic equation and κ is the apparent rate of the pseudo-first-order reaction, according to equations (2) and (3) (Konstantinou and Albanis, 2004):

$$-r_i = -\frac{dC_i}{dt} = \kappa_S . K . C_i \quad (2)$$

$$\ln\left(\frac{C_{io}}{C_i}\right) = \kappa_S . K . t = \kappa . t \text{ or } C_i = C_{io} . e^{-\kappa t} \quad (3)$$

Pseudo first-order reaction rate constant was determined from the slope of the linear regression of ln(Co Ci^{-1}) *versus* time.

2.7 Statistical analysis

The SPSS Statistical System (SPSS for Windows, version 19,IBM®) was used to analyze the relationships among thedata. All statistical tests were performed at the $p<0.05$level of significance. The Spearman correlation coefficient(r_p) was used as a non-parametric measure of statisticaldependence between two variables, without making anyassumptions about the frequency distribution of thevariables.

III. RESULTS AND DISCUSSION

3.1 Catalyst characterization

xA.C. and the photocatalysts doped with titanium (xTi-A.C.) were characterized by scanning electron microscopy (SEM), diffuse reflectance spectroscopy in the ultraviolet (DRS-UV), nitrogen porosimetry and zeta potential (ZP) measurements. SEM was used for morphological analysis. For textural analysis of the catalyst, nitrogen porosimetry and zeta potential measurements were used. DRS-UV was used to evaluate the structural properties of the catalysts. Table 3 shows the results of analysis for the characterization of the photocatalysts. For comparative, the results of the commercial catalyst P25 were also determined.

https://dx.doi.org/10.22161/ijaers.6.2.20 *ISSN: 2349-6495(P) | 2456-1908(O)*

*Table.3: Results of the surface area (S_{BET}), pore diameter (Dp), pore volume (Vp), band gap energy (Eg), absorption wavelength (λ) and zeta potential (ZP) of the Evonik Aeroxide P25, activated charcoal prepared from vegetable sponge a*nd doped with Ti^{+4}

Sample	P25	SucGly-A.C.	Suc-A.C.	UreGly-A.C.	SucGlyTi-A.C.	SucTi-A.C.	UreGlyTi-A.C.
S_{BET} (m^2 g^{-1})	56	138.42	17.81	70.80	634.51	174.23	326.56
Dp (nm)	4.8	16.36	3.2	2.40	19.95	3.51	5.23
Vp (cm^3 g^{-1})	0.07	0.057	0.0014	0.042	0.32	0.002	0.078
λ (nm)	371.25	220.64	150.67	184.25	441.28	375.76	410.60
Eg (eV)	3.34	5.62	8.23	6.73	2.81	3.30	3.02
ZP (mV)	-24.0	-26.48	-6.66	-24.75	-35.30	-12.20	-33.00

According to Table 3, the samples xA.C. and xTi-A.C. showed higher specific surface area if compared to commercial P25. Furthermore, the samples SucGlyTi-A.C. and UreGlyTi-A.C.had energy gap (Eg) values lower than that of P25 and a higher zeta potential (in module) than the commercial catalyst. For photocatalysis, crystal structure, surface area and porosity are some of the factors that influence the photocatalytic performance. These factors are crucial in the production of electron/hole pairs, adsorption processes and also in the processes of oxidation-reduction (Cheng *et al.*, 2016). A high surface area to promote adsorption of the pollutant to be degraded on the catalyst/support surface, and a significant pore volume to allow diffusion of the pollutant to the catalyst center (Bet-Moushoul *et al.*, 2016).

The energy band gap (Eg) is a relevant parameter for the photocatalytic process, since the smaller the Eg, the less radiation energy is required to the activation of the process, which in turn may reach the visible light region and the values were calculated by using the formula E = hc/λ, where h is Plank's constant, c is the velocity of light and λ is the wavelength. The band gap of xA.C. and xTi–A.C. were found between 2.81 and 8.23 eV. The band gap of Ti^{+4} doped xA.C. was shifted slightly towards longer wavelength region. This is possibly due to the fact that, with titanium doping (Ti^{+4}), the concentration of the electron acceptor/donor species (e_{BC}^- and h_{BV}^+) increases, followed by a decrease in the polarization of the O^{2-} ion in the conduction band. Thus, it promotes a change in conduction bands and valence band levels, promoting a reduction in the energy band range of photocatalysts (Vadivel and Rajarajan, 2015).

Measurement of the zeta potential (ZP) is also an important tool for evaluating the surface charge distribution and stability of photocatalysts because compatibility between the surface potential and the charge of the molecule to be degraded may improve the photocatalytic activity (Gaya and Abdullah, 2008). According to Table 3, the samples xA.C and xTi-A.C. exhibited a negative surface potential that ranged from -6.66 to -35.30 mV. However, the samples doped with titanium showed a greater potential (in module), confirming that the surface doped with $TiO_2$is beneficialto the surface charge, according the Figure 1. Moreover, RhB is characterized by their cationicnature, and the compatibility between the surface potential of the photocatalyst and the charge of the molecule to bedegraded can improve the photocatalytic activity (Debrassi*et al.*, 2011; Salleh*et al.*, 2011), since the RhB dye tends to adsorb on the catalytic surface of the photocatalysts by attractive forces, thus allowing degradation of the pollutant.

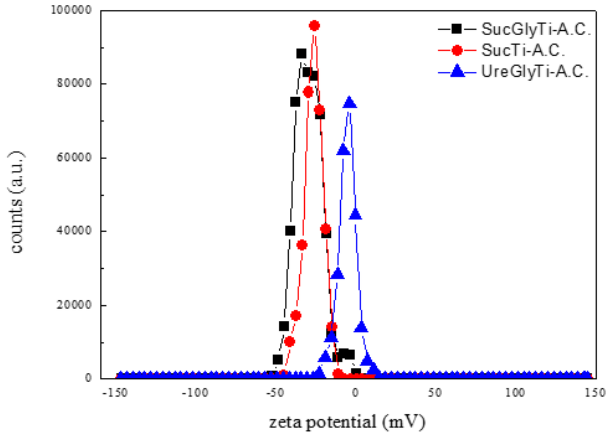

Fig.1: Zeta potential of the photocatalysts doped with Ti^{+4}.

Figure 2 shows some typical isotherms of adsorption/desorption of N_2 at 77 K which provides the indications of the presence of the pore size and structure. The isotherms are type IV sorption with a H3 hysteresis loop, according to IUPAC classification (IUPAC 1972), which indicates the existence of mesoporous in the corresponding materials and the type H4 loop is associated with narrow slit-like pores. The adsorption branch exhibits three distinct regions corresponding to a monolayer-multilayer adsorption, multilayer adsorption on the outer particle surfaces and capillary condensation at relative pressures in the range from 0.6 to 0.9, for all the isotherms. The Ti^{+4} sample showed the highest

https://dx.doi.org/10.22161/ijaers.6.2.20 *ISSN: 2349-6495(P) | 2456-1908(O)*

specific surface area and pore volume. Table 3 shows the characteristics of the resulting photocatalysts. For photocatalysis, one relevant strategy to enhance degradation is to guarantee high surface area of the catalyst to promote adsorption of the pollutant to be degraded on the catalyst/support surface, and a significant pore volume to allow diffusion of the pollutant to the catalyst center (Wang*et al.*, 2008). Then, a stable, high surface area with a three-dimensional mesoporous structure can achieve much facile adsorption/desorption equilibrium and mass diffusion of reactants and products and thus enhance the activity and stability of the Ti^{+4} material in the photocatalytic application.

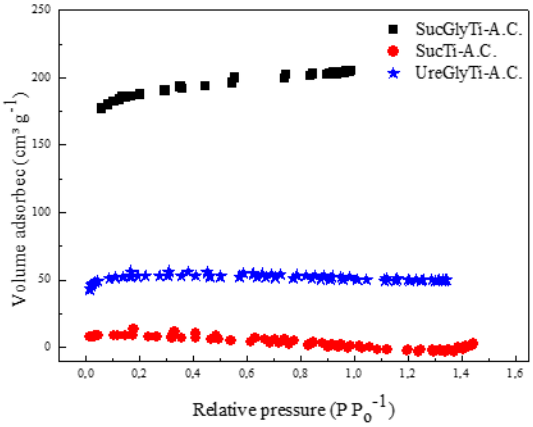

Fig.2: Nitrogen adsorption / desorption isotherms for the samples doped with Ti^{+4}.

According to Table 3, the sample SucGlyTi-A.C. showed higher S_{BET} value (634.51 m^2 g^{-1}) and higher porosity with 19.95 nm and 0.32 cm^3 g^{-1} diameter and pore volume, respectively. Among the doped samples, the presence of Ti^{+4} provided a significant increase in the surface area and porosity of the samples, for example the SucGlyTi-A.C. sample showed an increase of about 358% in its surface area, 22% in Dp and 461% in Vp. In addition, through the pore diameter, it is possible to affirm that they are structures with mesoporous (2-50 nm) (IUPAC, 1972) and, by the distribution of pores, it was possible to verify that SucGlyTi-A.C. showed a larger pore volume, followed by the UreGlyTi-A.C

Figures 3a and 3c show micrographs of the samples SucGlyTi-A.C and UreGlyTi-A.C., where it is possible to visualize a more dispersed distribution of the particles. Meanwhile, Figure 3b shows a micrograph of the SucTi-A.C sample indicating the formation of particle agglomerates (clusters). This can be explained by the surface charge (zeta potential), where the samples prepared with sucrose and glycine have higher repulsive forces between the particles, by the higher value of ZP, so the particles tend to disperse. While using only sucrose, the ZP is smaller between the particles, providing a lower dispersion and, thus, a greater sinterization of the particles, after calcination. In addition, this higher dispersion of the particles provides a higher catalytic surface area and thus a better adsorption of the target molecule and better photocatalytic activity (Kaleji*et al.*, 2011).

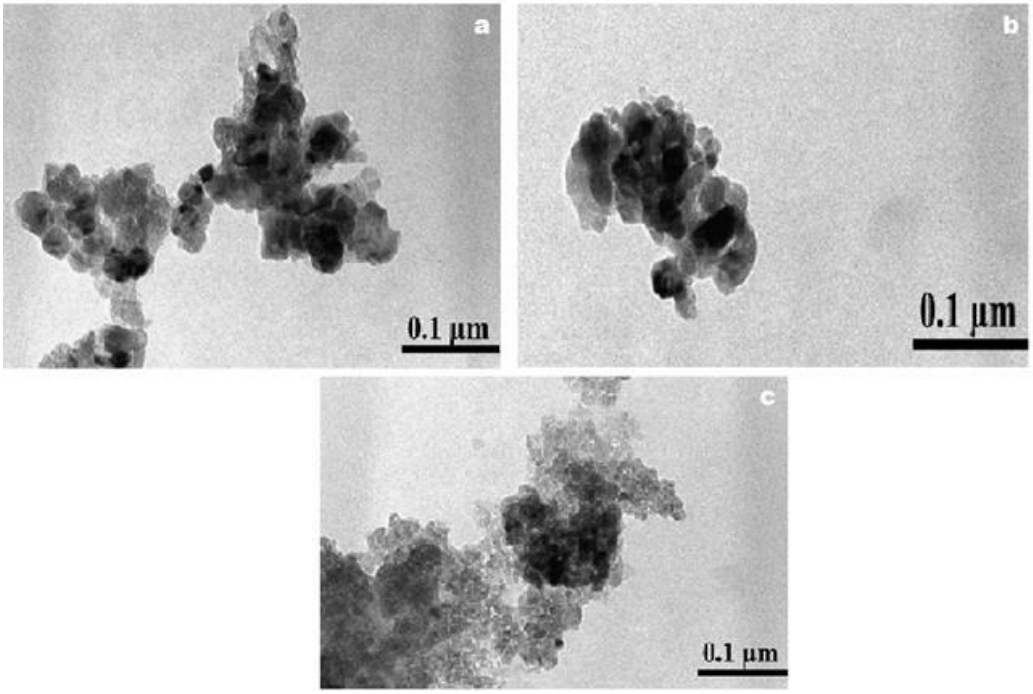

Fig.3: SEM images for the samples: (a) SucGlyTi-A.C., (b) SucTi-A.C., and (c) UreGlyTi-A.C.

3.2 Photocatalytic Activity

https://dx.doi.org/10.22161/ijaers.6.2.20 *ISSN: 2349-6495(P) | 2456-1908(O)*

Figure 4 shows the photocatalytic activity and the respective specific rates of reaction (k), under ultraviolet radiation, while Figure 5 under visible radiation, after 120 minutes of reaction of degradation of RhB dye. Moreover, adsorption results were added, indicating an adsorption of about 10% in the synthesized samples.

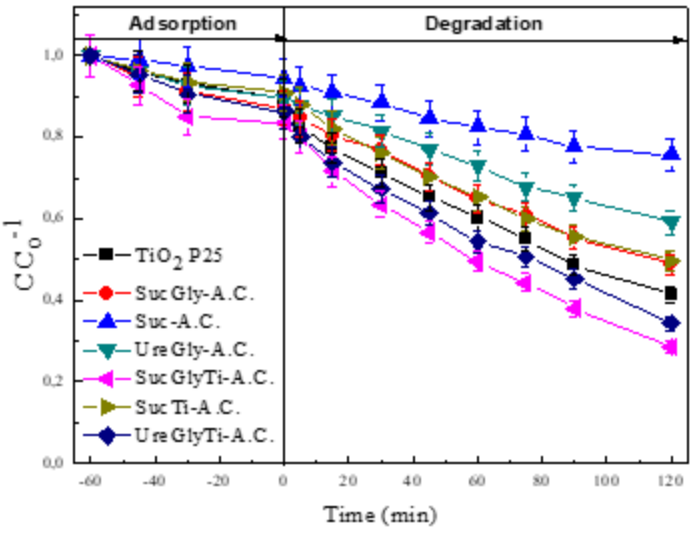

(a)

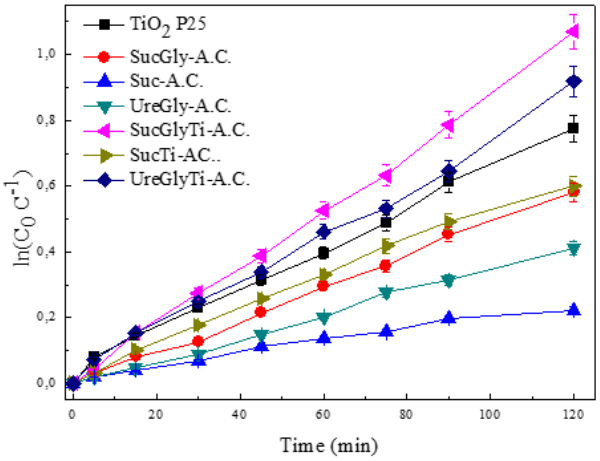

(b)

Fig.4: (a) Photocatalytic activity and (b) specific rate of the RhB dye degradation reaction of the samples synthesized under UV radiation after 120 minutes($C_{catalyst}$ = 0.7 g L^{-1}, C_{RhB} = 20 mg L^{-1}, T = 30 ° C, natural pH, UV radiation of 61.8 W m^{-2} and error 5%)

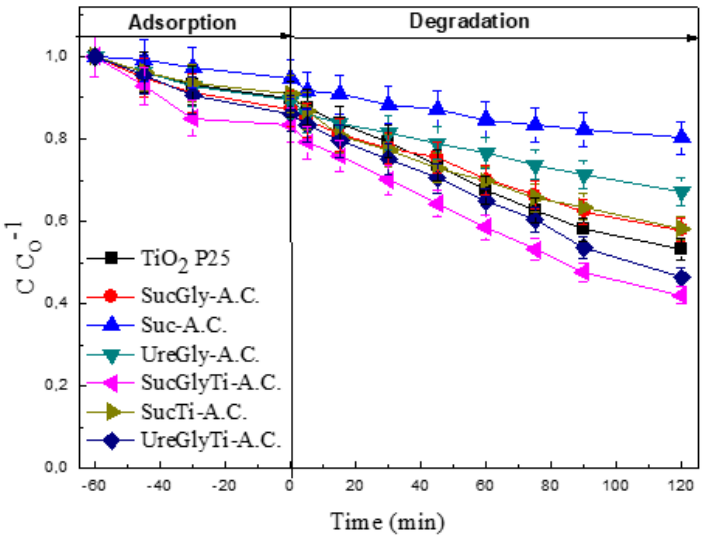

https://dx.doi.org/10.22161/ijaers.6.2.20 *ISSN: 2349-6495(P) | 2456-1908(O)*

(a)

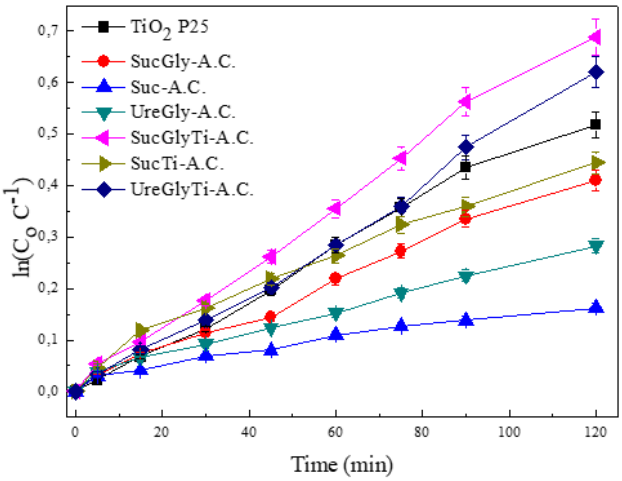

(b)

Fig.5: (a) Photocatalytic activity and (b) specific rate of the RhB dye degradation reaction of the samples synthesized under visible radiation after 120 minutes ($C_{catalyst}$ = 0.7 g L^{-1}, C_{RhB} = 20 mg L^{-1}, T = 30 ° C, natural pH, visible radiation of 202 W $m^{-2}$and error 5%)

Under ultraviolet radiation (Figure 4), the photolysis of RhB represents about 14% of the degradation and the SucGlyTi-A.C. (66 %) showed the best activity photocatalytic, which can be justified according its structural and structural characteristics, such as higher surface area (S_{BET}) and porosity (Dp and Vp), lower band gap energy (Eg) and higher load (ZP, in module), providing a better mass transfer and diffusion of the RhB molecules and, thus, a better photocatalytic activity. Moreover, all doped samples showed a significant increase in degradation of about 49 %, 127 % and 78 % for the SucGlyTi-A.C. (k = 0.0088 min^{-1}), SucTi-A.C. (k = 0.0053 min^{-1}) and UreGlyTi-A.C. (k = 0.0075 min^{-1}), relative to the non-doped samples, SucGly-A.C. (k = 0.0049 min^{-1}), Suc-A.C. (k = 0.0021 min^{-1}) and UreGly-A.C. (k = 0.0049 min^{-1}). In relation to the commercial catalyst (TiO_2 P25), SucGlyTi-A.C. and UreGly-A.C. obtained a superior catalytic performance under UV radiation, that is, while TiO_2 showed a degradation of 53.92% after 120 minutes of reaction, the same 65.71 % and 60.10 % respectively under the same conditions.

While under visible radiation (Figure 5), photolysis represents 4 % degradation, in addition to the samples SucGlyTi-A.C. (49.8% and k = 0.0059 min^{-1}), SucTi-A.C. (35.9% and k = 0.0041 min^{-1}) and UreGlyTi-A.C. (46.25% e k = 0.0050 min^{-1}) showed an increase in their photocatalytic activity after Ti^{+4} doping (48 %, 139 % and 87 % in relation to SucGly-A.C., Suc-A.C. and UreGly-A.C. , respectively), highlighting for the photocatalyst SucGlyTi-A.C. which, as in ultraviolet radiation, showed a higher photocatalytic activity. In all degradation processes, the reactions followed a pseudo-first order kinetics. Table 4 shows the respective values of the specific reaction rate (k) and photocatalytic degradation.

Table.4: Specific reaction rates (k) of the RhB tests under UV and visible radiation

Catalyst	% degradation (UV)	k_{UV} (min^{-1})	% degradation (vis)	k_{vis} (min^{-1})
TiO_2 P25	53.9	0.0067	40.4	0.0046
SucGly-A.C.	44.1	0.0049	33.6	0.0036
Suc-A.C.	19.9	0.0021	15.0	0.0016
UreGly-A.C.	33.8	0.0035	24.7	0.0025
SucGlyTi-A.C.	66.0	0.0088	49.8	0.0059
SucTi-A.C.	45.1	0.0053	35.9	0.0041
UreGlyTi-A.C.	60.1	0.0075	46.2	0.0050

Some strong Spearman's correlations were observed between some electronic and physical properties, as illustrated in Figures 6, 7 and 8. It was possible to observe a strong direct correlation between the specific surface area (S_{BET}) and specific reaction rates (k) underUV (r_p> 0.941) and visible (r_p> 0.919) radiation (Figure 6), as well as an indirect correlation between band gap energy (Eg) (r_p< - 0.920 to UV radiation and r_p< - 0.952 to visible radiation) and zeta potential (ZP) (r_p< - 0.798 to UV radiation and r_p< - 0.749 to visible radiation) with the specific reaction rates (k), according to Figure 7 and 8, respectively . Thus, the higher the surface area, the greater the amount of RhB adsorbed and thus the greater the degradation and the reaction rate. On the other hand,

https://dx.doi.org/10.22161/ijaers.6.2.20 *ISSN: 2349-6495(P) | 2456-1908(O)*

the higher the Eg and ZP, the greater the energy required to activate the catalyst and the larger the surface repulsive forces, so the catalytic efficiency will be lower, affecting the rate of reaction.

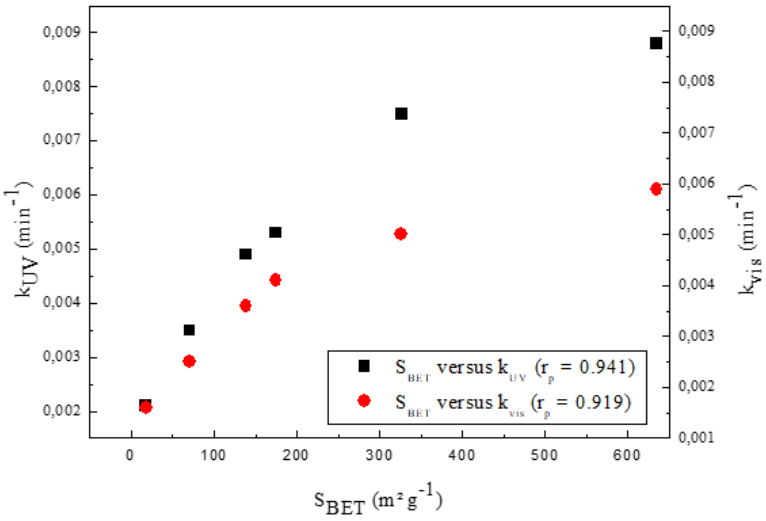

Fig.6: Correlation between specific surface area (S_{BET}) and specific reaction rates (k).

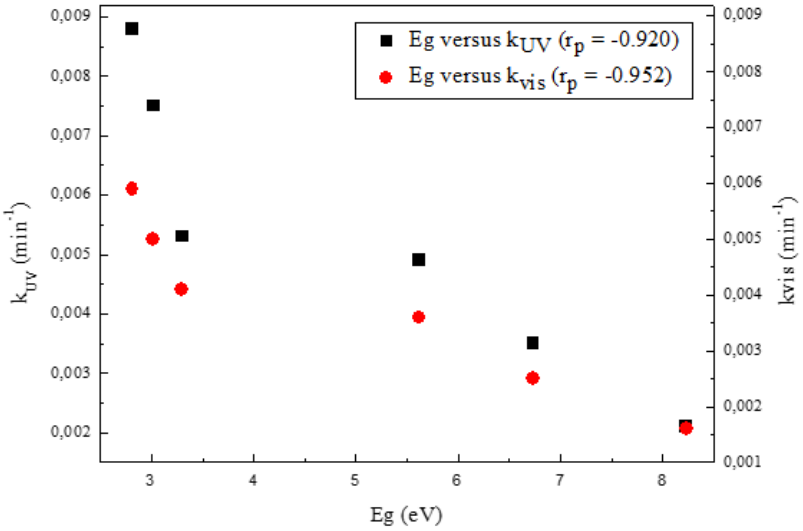

Fig.7: Correlation between band gap energy (Eg) and specific reaction rates (k).

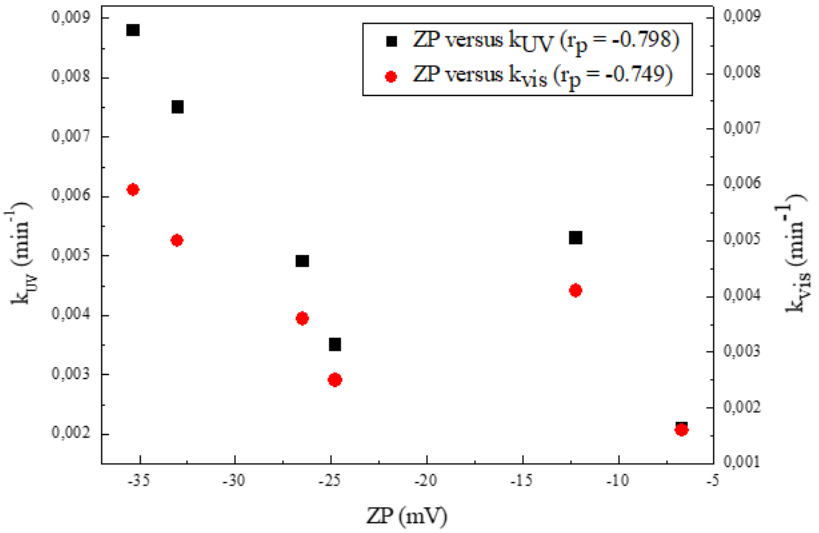

Fig.8: Correlation between zeta potential (ZP) and specific reaction rates (k).

https://dx.doi.org/10.22161/ijaers.6.2.20 *ISSN: 2349-6495(P) | 2456-1908(O)*

IV. CONCLUSION

In summary, it can be concluded that the photo degradation kinetics of the Rhoda mine B dye can be approximated to a pseudo-order model and that the doping with Ti^{+4} provided changes in the textural and structural properties, in relation to the non-doped samples, such as band gap energy (Eg), surface area (S_{BET}), porosity (Dp and Vp), zeta potential (ZP), and a better photocatalytic performance in the degradation of RhB dye, under UV and visible radiation. Moreover, these results suggest that the positive effect of titanium as a dopant in the development of photocatalysts, due to the fact that Ti^{+4} is capable of generating an intermediate band gap energy between the conduction and valence bands of the non-doped sample, capable of promoting the absorption of photons and generating more electron / vacancy pairs (e_{BC}^- and h_{BV}^+) and, thus, providing a higher formation of the hydroxyl radical (•OH). Therefore, photocatalysts doped with titanium from activated charcoal prepared with vegetable sponge are promising for use in the degradation of organic pollutants, via heterogeneous photocatalysis.

ACKNOWLEDGMENTS

The authors would thank to Laboratory of Catalysis and Polymers (K106) and Federal University of Rio Grande do Sul (UFRGS) for the support and assistance to present work.

REFERENCES

[1] Abed C, Bouzidi C, Elhouichet H, Gelloz B, Ferid M (2015) Mg doping induced high structural quality of sol–gel ZnO nanocrystals: Application in photocatalysis. Applied Surface Science 349:855–863.https://doi.org/10.1016/j.apsusc.2015.05.078.

[2] Almeida CMVB, Frimaio GS, Bonilla SH, da Silva CC, Giannetti BF (2012) An evaluation of a MSW-to-energy system using eMergy synthesis. International Journal of Environment and Sustainable Development 11:258–73. http://dx.doi.org/10.1504/IJESD.2012.050462.

[3] Barros BS, Melo PS, Gama L, Alves JRS, Fagury-Neto E, Kiminami RHGA, Costa ACFM (2005) Luminescence and morphology of zinc aluminate doped with Eu^{3+} nanoparticles. Cerâmica 51:63-69. http://dx.doi.org/10.1590/S0366-69132005000100012.

[4] Bet-MoushoulE, MansourpanahY, FarhadiK, TabatabaeiM (2016) TiO_2 nanocomposite based polymeric membranes: A review on performance improvement for various applications in chemical engineering processes. Chemical Engineering Journal283:29–46. https://doi.org/10.1016/j.cej.2015.06.124.

[5] ChengM, ZengG, HuangD, LaiC, XuP, ZhangC, LiuY (2016) Hydroxyl radicals based advanced oxidation processes (AOPs) for remediation of soils contaminated with organic compounds: A review. Chemical Engineering Journal 284:582–598. https://doi.org/10.1016/j.cej.2015.09.001.

[6] DebrassiA, CorrêaA, BaccatinT, NedelkoN **(**2011**)** Removal of cationic dye from aqueous solution using N-benzyl-O-carboxymethylchitosan magnetic nanoparticles. Chemical Engineering Journal 183**:**284-293. https://doi.org/10.1016/j.cej.2011.12.078.

[7] DunnPJ (2012) The importance of green chemistry in process research and development. Chemical Society Review 41:1452-1461. https://doi.org/10.1039/C1CS15219J.

[8] GayaUI, AbdullahAH (2008) Heterogeneous photocatalytic degradation of organic contaminants over titanium dioxide: A review of fundamentals, progress and problems. Journal of Photochemistry and Photobiology C: Photochemistry Reviews 9:1-12.https://doi.org/10.1016/j.jphotochemrev.2007.12.003.

[9] HerrmannJM (2005) Heterogeneous photocatalysis: state of the art and presente application. Topics in Catalysis34:49-65. https://doi.org/10.1007/s11244-005-3788-2.

[10] IUPAC (1972) Manual of symbols and Terminology, Appendix 2, Part 1, Colloid and Surface Chemistry. Pure Apllied Chemical31:578-638.

[11] KalejiBK, Sarraf-MamooryR, SanjabiS (2011) Photocatalytic evaluation of a titania thin film on glazed porcelain substrates via a $TiCl_4$ precursor. Reaction Kinetics, Mechanisms and Catalysis103:289-298.https://doi.org/10.1007/s11144-011-0327-y.

[12] KonstantinouL,AlbanisT (2004) Photocatalytic transformation of pesticides in aqueous titanium dioxide suspensions using artificial and solar light: intermediates and degradation pathways. Applied Catalysis B: Environmental42:319-335. https://doi.org/10.1016/S0926-3373(02)00266-7.

[13] LinX, RongF, JiX, FuD (2011) Carbon-doped mesoporous TiO_2 film and its photocatalytic activity. Microporous and Mesoporous Materials 142:276-281. https://doi.org/10.1016/j.micromeso.2010.12.010.

[14] LiuH, WuY, ZhangJ (2011) A new approach toward carbon-modified vanadium-doped titanium dioxide photocatalysts. ACS Applied Materials & Interfaces 3:1757-1764. https://doi.org/10.1021/am200248q.

[15] MaJ, LiL, ZouJ, KongY, KomarneniS (2014) Highly efficient visible light degradation of rhodamine B by

nanophasic Ag_3PO_4 dispersed on SBA-15. Microporous and Mesoporous Materials 193:154-159. https://doi.org/10.1016/j.micromeso.2014.03.026.

[16] MourãoHAJL, De MendonçaVR (2009) Nanostructures in photocatalysis: a review about synthesis strategies of photocatalysts in nanometric size. Química Nova32:2181-2190. http://dx.doi.org/10.1590/S0100-40422009000800032.

[17] PereiraVJ, FernandesD, CarvalhoG, BenolielMJ, San RomãoMV, CrespoMTB (2010) Assessment of the presence and dynamics of fungi in drinking water sources using cultural and molecular methods. Water Resources 44:4850-4859. https://doi.org/10.1016/j.watres.2010.07.018.

[18] SallehMAM, MahmaoundDK, KarimWAWA, IdrisA (2011) Cationic and anionic dye adsorption by agricultural and solid wastes: A comprehensive review. Desalination 280:1-13. https://doi.org/10.1016/j.desal.2011.07.019.

[19] VadivelS, RajarajanC (2015) Effect of Mg doping on structural, optical and photocatalytic activity of SnO_2 nanostructure thin films. Journal of Material Science: Materials in Eletronics 26:3155-3162. https://doi.org/10.1007/s10854-015-2811-z.

[20] WangM, SongG, LiJ, MiaoL, ZhangB (2008) Direct hydrothermal synthesis and magnetic property of titanate nanotubes doped magnetic metal ions. Journal of University of Science and Technology Beijing 15:644-648. https://doi.org/10.1016/S1005-8850(08)60120-6.

[21] WuD, LongM, CaiW, ChenC, WuY (2010) Low temperature hydrothermal synthesis of N-doped TiO_2 photocatalyst with high visible-light activity, Journal of Alloys and Compounds 502:289-294. https://doi.org/10.1016/j.jallcom.2010.04.189.

[22] XuY, ZhuangY, FuX (2010) New insight for enhanced photocatalytic activity of TiO_2 by doping carbon nanotubes: a case study on degradation of benzene and methyl orange. The Journal of Physical Chemistry C114:2669-2676. https://doi.org/10.1021/jp909855p.

[23] ZhangH, LingC, LiuJ, TianZ, WangG, CaiW (2012) Defect-mediated formation of Ag cluster-doped TiO_2 nanoparticles for efficient photodegradation of pentachlorophenol. Langmuir28:3938-3944. https://doi.org/10.1021/la2043526.

FIGURE CAPTIONS

Figure 1. Zeta potential of the photocatalysts doped with Ti^{+4}.

Figure 2. Nitrogen adsorption / desorption isotherms for the samples doped with Ti^{+4}.

Figure 3. SEM images for the samples: (a) SucGlyTi-A.C., (b) SucTi-A.C., and (c) UreGlyTi-A.C.

Figure 4. (a) Photocatalytic activity and (b) specific rate of the RhB dye degradation reaction of the samples synthesized under UV radiation after 120 minutes ($C_{catalyst}$ = 0.7 g L^{-1}, C_{RhB} = 20 mg L^{-1}, T = 30 ° C, natural pH, UV radiation of 61.8 W m^{-2} and error 5%)

Figure 5. (a) Photocatalytic activity and (b) specific rate of the RhB dye degradation reaction of the samples synthesized under visible radiation after 120 minutes ($C_{catalyst}$ = 0.7 g L^{-1}, C_{RhB} = 20 mg L^{-1}, T = 30 ° C, natural pH, visible radiation of 202 W m^{-2} and error 5%)

Figure 6. Correlation between specific surface area (S_{BET}) and specific reaction rates (k)

Figure 7. Correlation between band gap energy (Eg) and specific reaction rates (k)

Figure 8. Correlation between zeta potential (ZP) and specific reaction rates (k)

TABLE CAPTIONS

Table 1. Compositions of activated charcoal (A.C.) in proportions

Table 2. Photocatalysts doped with Ti^{+4}

Table 3. Results of the surface area (S_{BET}), pore diameter (Dp), pore volume (Vp), *band gap* energy (Eg), absorption wavelength (λ) and zeta potential (ZP) of the Evonik Aeroxide P25, activated charcoal prepared from vegetable sponge and doped with Ti^{+4}

Table 4. Specific reaction rates (k) of the RhB tests under UV and visible radiation